



First-principles investigation of hydrous post-perovskite



Joshua P. Townsend^{a,*}, Jun Tsuchiya^b, Craig R. Bina^a, Steven D. Jacobsen^a

^a Department of Earth and Planetary Sciences, Northwestern University, Evanston, IL 60208, United States

^b Geodynamics Research Center, Ehime University, Matsuyama, Ehime 790, Japan

ARTICLE INFO

Article history:

Received 8 September 2014

Received in revised form 20 January 2015

Accepted 26 March 2015

Available online 11 April 2015

Keywords:

Hydrogen

Post-perovskite

Lower mantle

Elasticity

ABSTRACT

A stable, hydrogen-defect structure of post-perovskite (hy-ppv, $\text{Mg}_{1-x}\text{SiH}_2\text{xO}_3$) has been determined by first-principles calculations of the vibrational and elastic properties up to 150 GPa. Among three potential hy-ppv structures analyzed, one was found to be stable at pressures relevant to the lower-mantle D'' region. Hydrogen has a pronounced effect on the elastic properties of post-perovskite due to magnesium defects associated with hydration, including a reduction of the zero-pressure bulk (K_0) and shear (G_0) moduli by 5% and 8%, respectively, for a structure containing ~ 1 wt.% H_2O . However, with increasing pressure the moduli of hy-ppv increase significantly relative to ppv, resulting in a structure that is only 1% slower in bulk compressional velocity and 2.5% slower in shear-wave velocity than ppv at 120 GPa. In contrast, the reduction of certain anisotropic elastic constants (C_{ij}) in hy-ppv increases with pressure (notably, C_{55} , C_{66} , and C_{23}), indicating that hydration generally increases elastic anisotropy in hy-ppv at D'' pressures. Calculated infrared absorption spectra show two O–H stretching bands at ~ 3500 cm^{-1} that shift with pressure to lower wavenumber by about 2 $\text{cm}^{-1}/\text{GPa}$. At 120 GPa the hydrogen bonds in hy-ppv are still asymmetric. The stability of a hy-ppv structure containing 1–2 wt.% H_2O at D'' pressures implies that post-perovskite may be a host for recycled or primordial hydrogen near the Earth's core-mantle boundary.

© 2015 Elsevier B.V. All rights reserved.

1. Introduction

Seismic investigations of the lowermost several hundred kilometers of the mantle (called the D'' region) have revealed a heterogeneous region with large-scale structures including large low-shear-velocity provinces (LLSVPs) and ultralow-velocity zones (ULVZs) overlying the core (Garnero and McNamara, 2008). The bridgmanite (brg) to post-perovskite (ppv) phase transition of MgSiO_3 has been invoked to explain some of the features within the D'' region (Murakami et al., 2004; Tsuchiya et al., 2004; Oganov and Ono, 2004; Wookey et al., 2005; Nowacki et al., 2010). The composition and mineralogy of D'' remains unresolved due to uncertainties in core-mantle boundary (CMB) temperature (Nomura et al., 2014), spatial heterogeneity of D'' material (e.g. slab graveyards) (Garnero and McNamara, 2008), and the effect of major element substitution on physical properties of the brg/ppv phase boundary for candidate lower mantle compositions (Grocholski et al., 2012).

Previous studies have investigated the effect of major-element substitution on the bridgmanite to post-perovskite phase

transition and on physical properties of post-perovskite (Murakami and Hirose, 2005; Mao et al., 2006; Grocholski et al., 2012). In Al-free systems, increasing Fe^{2+} decreases the pressure of the phase boundary, whereas increasing Fe^{3+} and Al-content suppresses the phase boundary to higher pressures (greater depths) (Grocholski et al., 2012). The brg to ppv transition should occur above the CMB in harzburgite and MORB but potentially below the CMB conditions in pyrolite (Grocholski et al., 2012). However, the influence of hydrogen on ppv structure and physical properties has not been determined.

The bulk H_2O content of the mantle is among the least well constrained compositional parameters of the Earth, with estimates varying by orders of magnitude due to uncertainty in the bulk mantle and core hydrogen content (e.g. Williams and Hemley, 2001). The water storage capacity of the uppermost mantle varies with depth, but in the peridotite system olivine and pyroxene can contain about 0.1 wt.% H_2O at 400 km depth (Tenner et al., 2012; Ferot and Bolfan-Casanova, 2012). The transition zone water storage capacity is likely much higher because wadsleyite and ringwoodite can incorporate 1–2 wt.% H_2O into their structures (Bolfan-Casanova et al., 2000; Inoue et al., 2010; Kohlstedt et al., 1996). The recent discovery of a hydrous ringwoodite inclusion in diamond containing ~ 1.5 wt.% H_2O suggests the transition zone

* Corresponding author.

E-mail address: joshua@earth.northwestern.edu (J.P. Townsend).

may be very hydrous, at least locally (Pearson et al., 2014). The H₂O storage capacity of the lower mantle remains highly uncertain due to conflicting estimates of H₂O storage capacity of bridgmanite, which range from about 0.001 wt.% (Bolfan-Casanova et al., 2003) to 0.4 wt.% (Murakami et al., 2002) and values in between (Litasov et al., 2003). A recent computational investigation by Hernandez et al., 2013 calculated the hydrogen partition coefficient between ringwoodite, ferropericlase, and bridgmanite and estimated that bridgmanite may contain up to 1000 ppm (0.1 wt.%) water. Contrast in the H₂O storage capacity between ringwoodite and bridgmanite may lead to dehydration melting below the 660 km discontinuity and provide evidence for regional scale hydration of the transition zone (Schmandt et al., 2014).

In contrast to bridgmanite, the post-perovskite structure is potentially more accommodating of hydrogen because both oxygen sites of the structure are slightly under-bonded. Magnesium is coordinated to eight oxygens with interatomic distances less than 2 Å and to two oxygens with distances slightly longer than 2 Å (Zhang et al., 2013). If the two longer oxygens are excluded from the Pauling bond strength sum, both O1 and O2 have the potential to protonate with charge balance achieved by an Mg-site vacancy. To test the idea that ppv may store seismically detectable amounts of hydrogen at D'' pressures, we have investigated several potential hydrous post-perovskite structures using density functional theory (DFT). We describe the most favorable hy-ppv structure and calculate its elastic and vibrational properties under static conditions in order to determine its mechanical stability, single-crystal and bulk-elastic wave velocities, and infrared absorption spectra.

2. Methods

Post-perovskite is orthorhombic with space group *Cmcm* (Murakami et al., 2004; Tsuchiya et al., 2004; Oganov and Ono, 2004). The structure contains alternating layers of corner-sharing SiO₆ octahedra and Mg polyhedra in eight coordination to oxygen (Murakami et al., 2004; Zhang et al., 2013). DFT calculations were carried out using the PWSCF code, part of the Quantum ESPRESSO package using the Perdew–Ernzerhof–Burke generalized gradient approximation (Hohenberg, 1964; Kohn and Sham, 1965; Perdew et al., 1996; Giannozzi et al., 2009). Wavefunctions were expanded with plane waves using an energy cutoff of 100 Ry. Norm-conserving pseudopotentials were used to describe H, O, and Si (Troullier and Martins, 1991). The Mg pseudopotential was generated by the method of U. von Barth and R. Car and has been used in previous investigations of hydrogen in silicates (Karki and Wentzcovitch, 2000; Tsuchiya et al., 2004; Tsuchiya and Tsuchiya, 2009). A supercell consisting of 4x1x1 ppv unit cells (80–82 atoms) was used for all calculations. The irreducible

Brillouin zone was sampled on a 2 × 2 × 2 Monkhorst–Pack mesh (Monkhorst and Pack, 1976). Both plane-wave cutoff energy and mesh size were tested for adequate total energy convergence. Unit-cell parameters and atomic coordinates were simultaneously relaxed at 0 K with a force convergence criterion of 10^{−5} Ry/Bohr.

Because there are no experimental data available for hydrous ppv, H defects were created by introducing Mg-site vacancies, Mg_{1−x}SiH_{2x}O₃, as similar vacancy structures have been reported in other high-pressure silicates such as wadsleyite and ringwoodite (Tsuchiya and Tsuchiya, 2009; Kudoh and Inoue, 1999; Li et al., 2009; Ganskow et al., 2010; Verma and Karki, 2009). Coupled substitutions of Fe³⁺ or Al³⁺ and H⁺ for Si⁴⁺ may also be important in the ppv phase, but in this study we first consider only charge-balanced vacancy substitutions in which one magnesium atom from the ppv 4 × 1 × 1 supercell is replaced with two hydrogen atoms (Mg_{0.938}SiH_{0.125}O₃), corresponding to a concentration of approximately 1.14 wt.% H₂O. We also created a second structure in the same scheme as above, but with 2 magnesium vacancies and 4 hydrogens (Mg_{0.875}SiH_{0.250}O₃) corresponding to 2.31 wt.% H₂O. In the more hydrous model the magnesium vacancies were created such that the vacancies were far apart (>7 Å at 0 GPa) to minimize interactions between vacancies. The 9 single-crystal elastic components were obtained from calculations of total energy and stress for incrementally strained orthorhombic super-cells (Karki et al., 2001). The largest strain was 0.01 and was checked to ensure a linear response. The infrared spectrum of hy-ppv was calculated for several pressures at the Γ -point under 0 K conditions via density functional perturbation theory under the linear-response theory of Baroni et al., 2001, in which the dynamical matrix along with dielectric quantities such as the Born effective charge tensor are evaluated at the Γ -point. The scheme outlined above is similar to previous ab initio calculations of IR spectra for hydrous silicates (Karki and Wentzcovitch, 2000; Blanchard et al., 2009; Verma and Karki, 2009; Brodholt and Refson, 2000; Umemoto et al., 2011).

3. Results and discussion

Three potential OH-defect structures of post-perovskite were studied by positioning hydrogen in a magnesium vacancy of the ppv supercell using the electron localization function (Gibbs et al., 2003) to identify initial H positions. The first model (hy-ppv1) features one O1–H group and one O2–H group, the second (hy-ppv2) features two approximately symmetric O2–H groups, and the third model (hy-ppv3) features two asymmetric O2–H groups. After calculation of phonons and enthalpy under static conditions for all structures, the stable H-defect structure is hy-ppv3 (hereafter hy-ppv), which features two distinct asymmetric hydrogen bonds as O2–H groups oriented in a plane normal to the *a*-axis. The hy-ppv1 structure was rejected due to unstable phonon

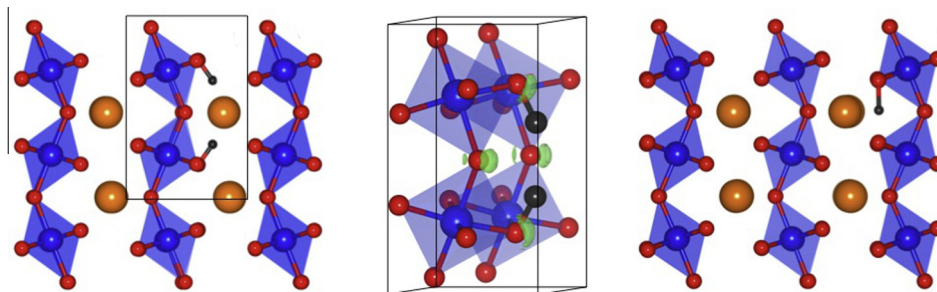


Fig. 1. Predicted stable hydrogen defect structure of hy-ppv at 120 GPa. Left: view of hy-ppv down the *a*-axis. Right: electron localization function 93-percentile iso-surface (green) of a Mg vacancy site in hy-ppv with super-imposed hydrogen groups. Atom positions are shown as oxygen (red), silicon (blue), magnesium (orange), and hydrogen (black). Lattice parameters and hydrogen-bond distances of the structure at 0 and 120 GPa are listed in Table 1. Fractional coordinates of atom positions for all structures are provided in the Supplementary materials. (For interpretation of the references to color in this figure legend, the reader is referred to the web version of this article.)

Table 1
Lattice parameters of ppv and hy-ppv at 0 and 120 GPa calculated in the current study. The hydrogen-bond geometry at 0 and 120 GPa is given for structures containing 1.14 and 2.31 wt.% H₂O. Structural information for ppv and hy-ppv at all pressures can be found in the [Supplementary materials](#).

Structure	<i>P</i> (GPa)	<i>a</i> (Å)	<i>b</i> (Å)	<i>c</i> (Å)	<i>V</i> (Å ³)	<i>E</i> (eV/FU)	<i>d</i> (O–H) (Å)	<i>d</i> (O···O) (Å)	<i>d</i> (H···O) (Å)	H-bond angle (°)
ppv	0	2.7020	9.1539	6.6966	165.6342	−1470.0485				
	120	2.4694	8.1039	6.1303	122.6800	−1466.8475				
hy-ppv (1.14 wt.%)	0	2.7079	9.1891	6.6867	166.3856	−1470.0176	0.9838	2.734	2.172	114.67
	120	2.4677	8.0965	6.1205	122.2835	−1466.8427	0.9928	2.306	1.707	114.74
hy-ppv (2.31 wt.%)	0	2.7173	9.2101	6.6744	167.0391	−1469.9448	0.9866	2.724	2.160	114.68
	120	2.4677	8.0808	6.1093	121.8254	−1466.6279	0.9977	2.297	1.693	114.78

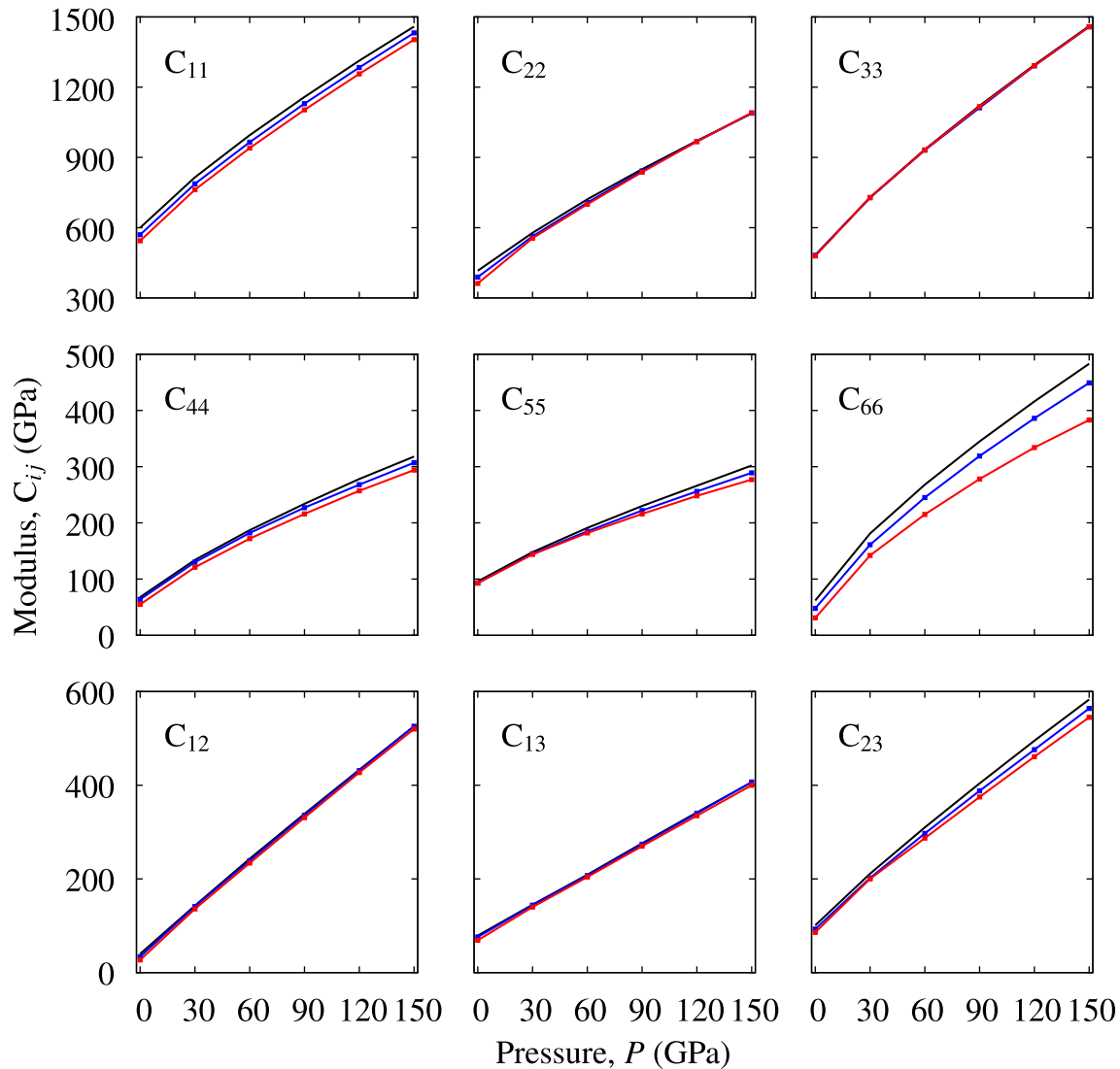


Fig. 2. Elastic tensor components (using Voigt notation) of ppv (black) and hy-ppv (1.14 wt.% H₂O in blue, 2.31 wt.% H₂O in red). *C*₂₂, *C*₃₃, *C*₁₂, and *C*₁₃ are relatively insensitive to hydration at all pressures, while *C*₁₁, *C*₄₄, *C*₅₅, *C*₆₆, and *C*₂₃ are more sensitive to hydration. At 120 GPa *C*₂₂ and *C*₃₃ are reduced by approximately 0.1% while *C*₆₆ is reduced by approximately 20% with addition of 2.31 wt.% H₂O. (For interpretation of the references to color in this figure legend, the reader is referred to the web version of this article.)

modes, and hy-ppv2, although stable, has a higher enthalpy than hy-ppv3 at 0 K at all pressures considered in this study (by about 0.10 eV per formula unit).

The stable structure of hy-ppv at 120 GPa is illustrated in Fig. 1. At 0 GPa, the O–H bond distance is 0.98 Å, with a hydrogen bond geometry of *d*(H···O) = 2.17 Å, *d*(O···O) = 2.73 Å, and hydrogen bond angle 115°. For comparison, the hydrogen-bond geometry in hydrous bridgmanite (Hernandez et al., 2013) is *d*(O–H) = 1.1 Å, *d*(H···O) = 1.65 Å, with a hydrogen-bond angle of about 150°. Thus, the hydrogen bond in hy-ppv is considerably more

non-linear than in hy-brg. In hy-ppv, the O–H bond distance increases slightly with pressure as the hydrogen bond distance *d*(O···O) shortens, consistent with general trends among hydrogen bonds in minerals (Libowitzky, 1999). Lattice parameters, energies, and hydrogen-bond geometry of hy-ppv at 0 and 120 GPa are listed in Table 1. Fractional coordinates of all the atom positions in all structures and all pressures are provided in the [Supplementary materials](#).

The effect of hydrogen on the elastic tensor of ppv is shown in Fig. 2. Generally *C*₄₄, *C*₅₅, *C*₆₆, and *C*₂₃ are most sensitive to

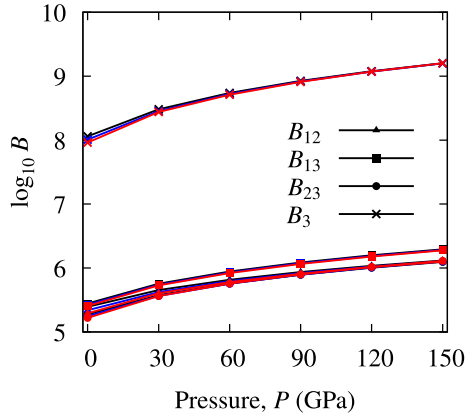


Fig. 3. Born stability criteria for ppv (black), and hy-ppv (1.14 wt.% H₂O in blue and 2.31 wt.% H₂O in red). Mechanical stability of the lattice requires each quantity be greater than zero. Addition of hydrogen to the ppv lattice does not destabilize the ppv structure. (For interpretation of the references to color in this figure legend, the reader is referred to the web version of this article.)

hydration, with the most sensitive component C_{66} reduced by 20% at 120 GPa for the 2.31 wt.% H₂O hy-ppv structure. We used the Born stability criteria to determine the mechanical stability of hy-ppv compared to ppv (Born and Huang, 1954). In the case of orthorhombic symmetry, these criteria reduce to the following:

$$B_{1,ii} = C_{ii} > 0 \quad (i = 1, 2, 3, \dots, 6) \quad (1)$$

$$B_{2,ij} = \det \begin{vmatrix} C_{ii} & C_{ij} \\ C_{ji} & C_{jj} \end{vmatrix} > 0 \quad (i, j = \{1, 2, 3\}, i \neq j) \quad (2)$$

$$B_3 = \det \begin{vmatrix} C_{11} & C_{12} & C_{13} \\ C_{21} & C_{22} & C_{23} \\ C_{31} & C_{32} & C_{33} \end{vmatrix} > 0 \quad (3)$$

The Born stability criteria calculated for pure ppv and hy-ppv are shown in Fig. 3 and indicate that hydrogen does not destabilize the post-perovskite lattice over lower mantle pressures for a simple Mg-2H substitution.

Bulk elastic properties for ppv and hy-ppv were calculated from the single-crystal elastic tensors using the Voigt–Reuss–Hill averaging scheme and are shown in Fig. 4 (Hill, 1952). The Hill-averaged elastic wave velocities decrease with hydration, as expected, but the bulk sound velocity (V_Φ) is remarkably insensitive to the presence of hydrogen. At 120 GPa, V_Φ is reduced by 8 m/s per wt.% H₂O (<0.1% decrease). In contrast to the bulk sound velocity, both the Hill-averaged P-wave (V_P) and S-wave (V_S) velocities decrease by approximately 68 m/s per wt.% H₂O (0.5% decrease) and 85 m/s per wt.% H₂O (1.1% decrease), respectively, at 120 GPa. Of particular note is that at 120 GPa the S-wave velocity of hy-ppv is slower than that of ppv and brg (for the 2.31 wt.% H₂O model), implying that a very hydrous hy-ppv, if present in D'', may be difficult to distinguish from bridgmanite using bulk sound velocity and/or shear-wave profiles alone.

The Hill averages of the bulk and shear moduli of ppv decrease linearly with water content, as shown in Fig. 5. At 0 GPa, the bulk modulus of ppv decreases by 9.6 GPa per wt.% H₂O, corresponding to 4.5% reduction per wt.% H₂O relative to the dry ppv $K_0 = 214$ GPa. The effect of water on the bulk modulus is significantly less at 120 GPa, with about 7.4 GPa reduction per wt.% H₂O, corresponding to only about 1% reduction in K per wt.% H₂O relative to the dry $K_{120} = 677$ GPa. In contrast, the shear modulus decreases by 9.3 GPa per wt.% H₂O at 0 GPa, corresponding to a

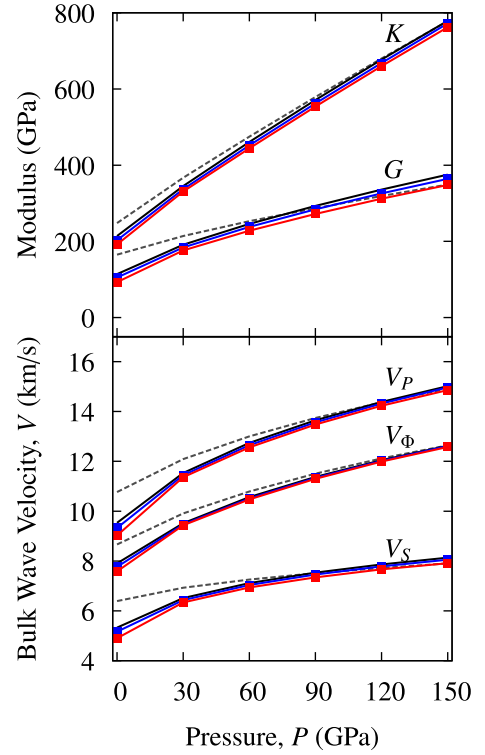


Fig. 4. Bulk elastic properties of brg (dashed), ppv (black), and hy-ppv (1.14 wt.% H₂O in blue, 2.31 wt.% H₂O in red). Voigt–Reuss–Hill averaged bulk modulus and shear modulus (top), and bulk wave velocities (bottom). Bulk sound velocity is relatively insensitive to hydrogen content, while bulk shear velocity is most sensitive. (For interpretation of the references to color in this figure legend, the reader is referred to the web version of this article.)

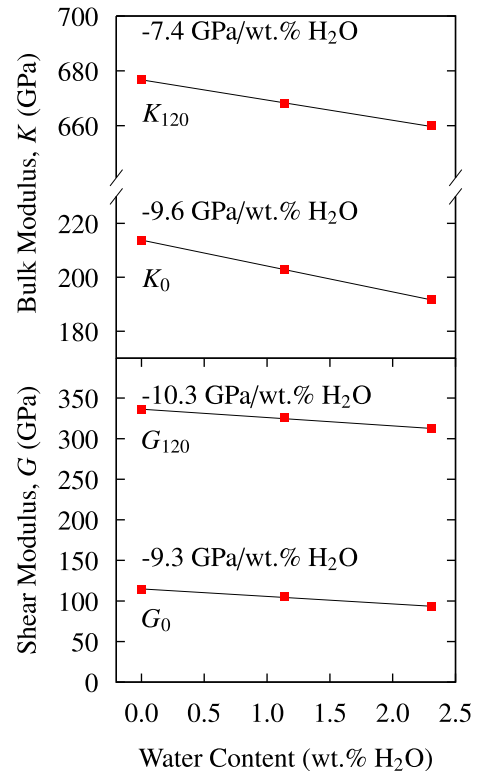


Fig. 5. Top: dependence of bulk modulus (top) and shear modulus (bottom) upon water content for ppv at 0 and 120 GPa.

Table 2
Pressure dependence of elastic properties, density, and Hill-averaged bulk wave velocities of ppv and hy-ppv. Elastic tensor, density, and elastic wave velocities at all pressures can be found in [Supplementary materials](#).

Structure	P (GPa)	C_{11} (GPa)	C_{22} (GPa)	C_{33} (GPa)	C_{44} (GPa)	C_{55} (GPa)	C_{66} (GPa)	C_{12} (GPa)	C_{13} (GPa)	C_{23} (GPa)	ρ (kg/m ³)	V_P (km/s)	V_S (km/s)	K (GPa)	G (GPa)
ppv	0	600	416	483	68	96	62	40	79	101	4025	9.54	5.33	214	114
	120	1313	971	1295	278	266	416	433	342	495	5435	14.38	7.86	677	336
hy-ppv (1.14 wt.%)	0	570	389	482	64	93	48	34	76	93	3951	9.32	5.16	203	105
	120	1284	968	1291	268	256	386	431	340	476	5375	14.32	7.78	668	326
hy-ppv (2.31 wt.%)	0	544	362	479	55	93	31	27	69	86	3880	9.03	5.16	192	93
	120	1257	968	1292	257	248	334	427	335	461	5320	14.23	7.66	660	312

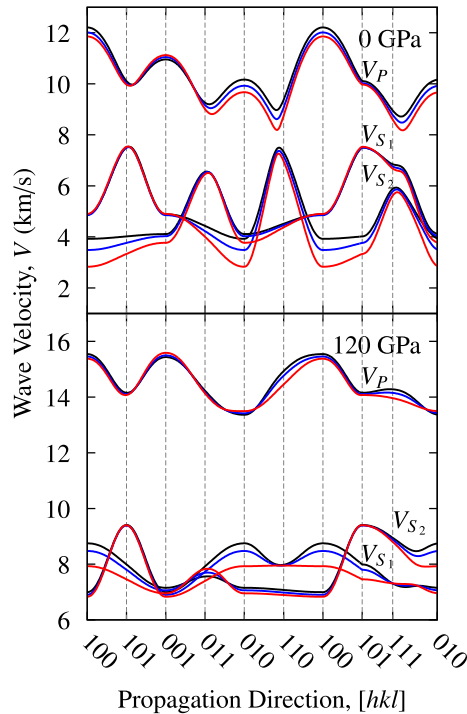


Fig. 6. Single crystal elastic wave velocities calculated for dry ppv (black), 1.14 wt.% H₂O (blue), and 2.31 wt.% H₂O (red). The presence of hydrogen has a pronounced effect on S-wave velocities relative to P-wave velocities. The presence of hydrogen does not noticeably change the minimum or maximum velocity directions. (For interpretation of the references to color in this figure legend, the reader is referred to the web version of this article.)

Table 3
Equation-of-state parameters of post-perovskite with varying hydrogen content. Bulk modulus (K_{T0}) and its pressure derivative (K'_{T0}) were fit using a 3rd-order Birch-Murnaghan equation of state.

Structure	K_{T0} (GPa)	K'_{T0}	V_{T0} (cm ³ /mol)
ppv	210	4.27	24.94
hy-ppv (1.14 wt.% H ₂ O)	201	4.28	25.05
hy-ppv (2.31 wt.% H ₂ O)	191	4.32	25.15

8.1% reduction per wt.% H₂O relative to the dry $G_0 = 114$ GPa. At 120 GPa, the shear modulus decreases by 10.3 GPa per wt.% H₂O, corresponding to about 3.1% reduction per wt.% H₂O relative to the dry $G_{120} = 336$ GPa. For comparison, the bulk modulus $K_0 = 203$ GPa for Mg hy-ppv containing ~1 wt.% H₂O is 25% lower than the $K_0 = 272$ GPa reported for anhydrous (Mg_{0.6}Fe_{0.4})-ppv (Mao et al., 2006). The reduction in K_0 (4.5%) and G_0 (8.1%) per wt.% H₂O for ppv upon hydration is about half that of ringwoodite, with about 7% reduction in K_0 and 15% reduction in G_0 per wt.%

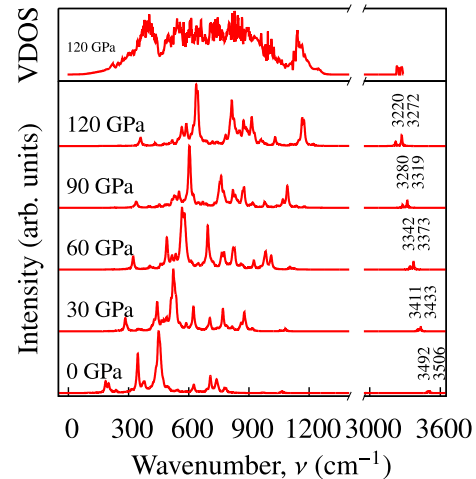


Fig. 7. Top: vibrational density of states for hy-ppv (1.14 wt.% H₂O) at 120 GPa. Bottom: calculated IR absorption spectra of hy-ppv at mantle pressures. Low-wavenumber peaks are lattice modes, and the two high-wavenumber peaks are characteristic of OH, representing in-phase stretching (low) and out-of-phase stretching (high).

H₂O (Jacobsen et al., 2004). However, one of the most important results of the current calculations is that at pressures of D'' , the calculated reduction by 1 wt.% H₂O in ppv is only about 1% in K and only about 3% in G , indicating that the hy-ppv structure is very stiff even in comparison with dry ppv. The combined influence of hydration, Al, and Fe-content in ppv remains to be explored in future work.

At D'' conditions, the effects of hydration on the Hill average of the bulk and shear moduli can be compared with the influence of temperature by applying the temperature derivatives of the moduli for ppv reported by Stackhouse et al., 2005. At 120 GPa, the influence of 1 wt.% H₂O on the bulk modulus is equivalent to raising the temperature by about 300 K, whereas the effect of 1 wt.% H₂O on the shear modulus is comparable to increasing temperature by about 675 K. There is very little effect of hydration on the V_P/V_S ratio of ppv, which shows about 0.01 increase (~0.5%) both at 0 and 120 GPa for 1 wt.% H₂O (Table 2).

The single crystal elastic wave velocities were calculated using the Cristoffel equation:

$$\det|c_{ijkl}n_k n_l - \rho V^2 \delta_{ij}| = 0 \quad (4)$$

where c_{ijkl} is the elastic tensor, n is the propagation direction, ρ is the density, V is the velocity and δ_{ij} is the Kronecker delta (Musgrave, 1970). The effect of H on the single crystal elastic wave velocities calculated from Eq. (4) at 0 and 120 GPa are shown in Fig. 6. The full elastic tensor and density at 0 and 120 GPa are listed in Table 2. At all pressures the presence of hydrogen reduces the elastic wave velocities for both P and S phases; however, the S-wave

velocities are more sensitive to hydration. At 120 GPa the single crystal V_p is generally unchanged by hydration while V_s is reduced by 1.2% per wt.% H_2O .

All ppv and hy-ppv structures were fit to 3rd-order Birch–Murnaghan equations of state (EOS), and EOS parameters are given in Table 3. At 0 GPa the addition of 1.14 wt.% H_2O increases the molar volume of ppv by 0.5%, and addition of 2.31 wt.% H_2O increases the molar volume by 0.9%. For comparison, the Mg end-member hydrous ringwoodite containing 2.2 wt.% H_2O studied by Inoue et al., 1998 had a molar volume 0.27% larger than dry Mg-ringwoodite (Weidner et al., 1984). Thus, at 0 GPa, the increase in molar volume due to hydration of ppv is about four times that of ringwoodite. However, due to the increased compressibility of the hy-ppv phase, at 120 GPa the 1.14 wt.% H_2O hy-ppv structure has a molar volume that is 0.3% smaller than dry ppv, and the 2.31 wt.% H_2O hy-ppv structure has a molar volume that is 0.7% smaller than dry ppv.

Calculated vibrational density of states and infrared absorption spectra of hy-ppv are shown in Fig. 7. Two O–H stretching bands are observed at 3492 and 3506 cm^{-1} at ambient pressure and correlate well with OH vibrational frequencies found in other high-pressure silicates (Libowitzky, 1999). With pressure these bands shift linearly with $dv_{3492}/dP = -2.25 cm^{-1}/GPa$ and $dv_{3506}/dP = -1.94 cm^{-1}/GPa$. In contrast to phase D we do not see hydrogen bond symmetrization in hy-ppv even at lower mantle pressures (Tsuchiya et al., 2005). The negative pressure shift of the OH modes is commonly observed in previous studies and occurs because the hydrogen bonds become more symmetric with increasing pressure which lengthens the O–H bond, thereby reducing the frequency (Libowitzky, 1999). The lower-frequency mode corresponds to in-phase stretching of the two OH groups, and the higher-frequency mode corresponds to 180-degree-out-of-phase stretching between the two OH groups. Measurements of OH in minerals at lower mantle pressures using current techniques is challenging, but experimental observation of OH in ppv may be especially challenging because ppv is not stable at low pressure (Mao et al., 2006), where many experimental measurements of OH in minerals are carried out.

4. Summary

Recent estimates of the return flux of water to the mantle via subduction suggest that perhaps several hundreds of ppm water may be retained in the slab beyond the depth of magma generation (Parai and Mukhopadhyay, 2012; Garth and Rietbrock, 2014). If slabs carry water through the lower mantle and into D'' , then ppv, the major silicate mineral in D'' , may be a potential host for water.

Primordial components, such as noble gases, in some ridge basalts may imply that magmas deriving from the deep mantle sample unmixed source regions (Craig et al., 1978; Gonnermann and Mukhopadhyay, 2007). The descent of slabs to the core mantle boundary (e.g. Garnero and McNamara, 2008) provides a mechanism of water incorporation into the D'' region, through both nominally anhydrous minerals and potential stability of dense hydrous magnesium silicates such as phase H to lower mantle conditions (Nishi et al., 2014). Though the equilibrium assemblage of hydrous minerals under lower mantle conditions is not well known, and we therefore cannot comment on the most likely host for water in D'' , this study has shown for the first time that a stable structure of hy-ppv persists to D'' pressures and displays modified elastic properties which may make it difficult to distinguish from brg using V_s profiles alone.

The stability of a hy-ppv structure containing 1–2 wt.% H_2O at D'' pressures implies that post-perovskite can potentially host a

significant amount of recycled or primordial hydrogen near the Earth's core–mantle boundary. Future research requires determination of the hydrogen partition coefficient between post-perovskite and other lower mantle phases such as bridgmanite, especially with more realistic compositions that include iron and aluminum. Further constraints on the effects of hydration on the mechanical and elastic properties of post-perovskite, especially at high temperature, will be important for future work that may provide insight into the fate of water in the seismically heterogeneous core–mantle boundary region.

Acknowledgements

JPT was supported by the EAPSI Program of the U.S. National Science Foundation (NSF) Grant Number 1209633 and the Japan Society for the Promotion of Science, and by the Premier Research Institute for Ultrahigh-pressure Sciences (PRIUS) joint research program carried out at the Geodynamics Research Center, Ehime University. This research was supported by NSF Grants EAR-1452344 (SDJ), EAR-0847951 (CRB), the Carnegie/DOE Alliance Center (CDAC), the David and Lucile Packard Foundation, and by the Alexander Von Humboldt Foundation.

Appendix A. Supplementary data

Supplementary data associated with this article can be found, in the online version, at <http://dx.doi.org/10.1016/j.pepi.2015.03.010>.

References

- Baroni, S., de Gironcoli, S., Dal Corso, A., 2001. Phonons and related crystal properties from density-functional perturbation theory. *Rev. Mod. Phys.* 73, 515–562.
- Blanchard, M., Balan, E., Wright, K., 2009. Incorporation of water in iron-free ringwoodite: a first-principles study. *Am. Mineral.* 94, 83–89.
- Bolfan-Casanova, N., Keppler, H., Rubie, D.C., 2000. Water partitioning between nominally anhydrous minerals in the MgO–SiO₂–H₂O system up to 24 GPa: implications for the distribution of water in the Earth's mantle. *Earth Planet. Sci. Lett.* 182, 209–221.
- Bolfan-Casanova, N., Keppler, H., Rubie, D.C., 2003. Water partitioning at 660 km depth and evidence for very low water solubility in magnesium silicate perovskite. *Geophys. Res. Lett.* 30, 1905.
- Born, M., Huang, K., 1954. *Dynamical Theory of Crystal Lattices*. Oxford University Press, London, U.K.
- Brodholt, J.P., Refson, K., 2000. An ab initio study of hydrogen in forsterite and a possible mechanism for hydrolytic weakening. *J. Geophys. Res.* 105, 18977–18982.
- Craig, H., Lupton, J.E., Welhan, J.A., Poreda, R., 1978. Helium isotope ratios in Yellowstone and Lassen park volcanic gases. *Geophys. Res. Lett.* 5, 897–900.
- Ferrot, A., Bolfan-Casanova, N., 2012. Water storage capacity in olivine and pyroxene to 14 GPa: implications for the water content of the Earth's upper mantle and nature of seismic discontinuities. *Earth Planet. Sci. Lett.* 349–350, 218–230.
- Ganskow, G., Boffa-Ballaran, T., Langenhorst, F., 2010. Effect of iron on the compressibility of hydrous ringwoodite. *Am. Mineral.* 95, 747–753.
- Garnero, E.J., McNamara, A.K., 2008. Structure and dynamics of Earth's lower mantle. *Science* 320, 626–628.
- Garth, T., Rietbrock, A., 2014. Order of magnitude increase in subducted H₂O due to hydrated normal faults within the Wadati–Benioff zone. *Geology* 42, 207–210.
- Giannozzi, P. et al., 2009. QUANTUM ESPRESSO: a modular and open-source software project for quantum simulations of materials. *J. Phys.: Condens. Matter* 21, 395502.
- Gibbs, G.V., Cox, D.F., Boisen Jr., M.B., Downs, R.T., Ross, N.L., 2003. The electron localization function: a tool for locating favorable proton docking sites in the silica polymorphs. *Phys. Chem. Miner.* 30, 305–316.
- Gonnermann, H.M., Mukhopadhyay, S., 2007. Non-equilibrium degassing and a primordial source for helium in ocean-island volcanism. *Nature* 449, 1037–1040.
- Grocholski, B., Catali, K., Shim, S.-H., Prakapenka, V., 2012. Mineralogical effects on the detectability of the postperovskite boundary. *Proc. Natl. Acad. Sci.* 109, 2275–2279.
- Hernandez, E.R., Alfe, D., Brodholt, J., 2013. The incorporation of water into lower-mantle perovskites: a first-principles study. *Earth Planet. Sci. Lett.* 364, 37–43.
- Hill, R., 1952. The elastic behavior of a crystalline aggregate. *Proc. Phys. Soc. A* 65, 349–354.
- Hohenberg, P., 1964. Inhomogeneous electron gas. *Phys. Rev.* 136, B864–B871.
- Inoue, T., Wada, T., Sasaki, R., Yurimoto, H., 2010. Water partitioning in the Earth's mantle. *Phys. Earth Planet. Inter.* 183, 245–251.

- Inoue, T., Weidner, D., Northrup, P., Parise, J., 1998. Elastic properties of hydrous ringwoodite (γ -phase) in Mg_2SiO_4 . *Earth Planet. Sci. Lett.* 160, 107–113.
- Jacobsen, S.D., Smyth, J.R., Spetzler, H., Holl, C.M., Frost, D.J., 2004. Sound velocities and elastic constants of iron-bearing hydrous ringwoodite. *Phys. Earth Planet. Inter.* 143–144, 47–56.
- Karki, B.B., Stixrude, L., Wentzcovitch, R.M., 2001. High-pressure elastic properties of major materials of earth's mantle from first principles. *Rev. Geophys.* 39, 507–534.
- Karki, B.B., Wentzcovitch, R.M., 2000. Ab initio lattice dynamics of MgSiO_3 perovskite at high pressure. *Phys. Rev. B* 62, 750–756.
- Kohlstedt, D., Keppler, H., Rubie, D., 1996. Solubility of water in the α , β and γ phases of $(\text{Mg}, \text{Fe})_2\text{SiO}_4$. *Contrib. Miner. Petrol.* 123, 345–357.
- Kohn, W., Sham, L.J., 1965. Self-consistent equations including exchange and correlation effects. *Phys. Rev.* 140, A1133–A1138.
- Kudoh, Y., Inoue, T., 1999. Mg-vacant structural modules and dilution of the symmetry of hydrous wadsleyite, $\beta\text{-Mg}_{2-x}\text{SiH}_{2x}\text{O}_4$ with $0.00 \leq x \leq 0.25$. *Phys. Chem. Miner.* 26, 382–388.
- Li, L., Brodholt, J., Alfe, D., 2009. Structure and elasticity of hydrous ringwoodite: a first principle investigation. *Phys. Earth Planet. Inter.* 177, 103–115.
- Libowitzky, E., 1999. Correlation of O–H stretching frequencies and O–HO hydrogen bond lengths in minerals. *Monatshefte Chem.* 130, 1047–1059.
- Litasov, K., Ohtani, E., Langenhorst, F., Yurimoto, H., Kubo, T., Konda, T., 2003. Water solubility in Mg-perovskites and water storage capacity in the lower mantle. *Earth Planet. Sci. Lett.* 211, 189–203.
- Mao, W.L., Mao, H.-K., Prakapenka, V.B., Shu, J., Hemley, R.J., 2006. The effect of pressure on the structure and volume of ferromagnesian post-perovskite. *Geophys. Res. Lett.* 33, L12S02.
- Monkhorst, H.J., Pack, J.D., 1976. Special points for Brillouin-zone integrations. *Phys. Rev. B* 13, 5188–5192.
- Murakami, M., Hirose, K., 2005. Post-perovskite phase transition and mineral chemistry in the pyrolytic lowermost mantle. *Geophys. Res. Lett.* 32, L03304.
- Murakami, M., Hirose, K., Kawamura, K., Sata, N., Ohishi, Y., 2004. Post-perovskite phase transition in MgSiO_3 . *Science* 304, 855–858.
- Murakami, M., Hirose, K., Yurimoto, H., Nakashima, S., Takafuji, N., 2002. Water in Earth's lower mantle. *Science* 295, 1885–1887.
- Musgrave, M.J.P., 1970. *Crystal Acoustics*. Holden-Day, Boca Raton, FL, USA.
- Nishi, M., Irifune, T., Tsuchiya, J., Tange, Y., Nishihara, Y., Fujino, K., Higo, Y., 2014. Stability of hydrous silicate at high pressures and water transport to the deep lower mantle. *Nat. Geosci.* 7, 224–227.
- Nomura, R., Hirose, K., Uesugi, K., Ohishi, Y., Tsuchiyama, A., Miyake, A., Ueno, Y., 2014. Temperature inferred from the solidus of pyrolite. *Science* 343, 522–525.
- Nowacki, A., Wookey, J., Kendall, J.-M., 2010. Deformation of the lowermost mantle from seismic anisotropy. *Nature* 467, 1091–1096.
- Oganov, A.R., Ono, S., 2004. Theoretical and experimental evidence for a post-perovskite phase of MgSiO_3 in earth's d layer. *Nature* 430, 445–448.
- Parai, R., Mukhopadhyay, S., 2012. How large is the subducted water flux? New constraints on mantle degassing rates. *Earth Planet. Sci. Lett.* 317–318, 396–406.
- Pearson, D.G., Brenker, F.E., Nestola, F., McNeill, J., Nasdala, L., Hutchison, M.T., Matveev, S., Mather, K., Silversmit, G., Schmitz, S., Vekemans, B., Vincze, L., 2014. Hydrous mantle transition zone indicated by ringwoodite included within diamond. *Nature* 507, 221–224.
- Perdew, J.P., Burke, K., Wang, Y., 1996. Generalized gradient approximation for the exchange-correlation hole of a many-electron system. *Phys. Rev. B* 54, 16533–16539.
- Schmandt, B., Jacobsen, S.D., Becker, T.W., Liu, Z., Ducker, K.G., 2014. Dehydration melting at the top of the lower mantle. *Science* 344, 1265–1268.
- Stackhouse, S., Brodholt, J., Wookey, J., Kendall, J.-M., Price, G., 2005. The effect of temperature on the seismic anisotropy of the perovskite and post-perovskite polymorphs of MgSiO_3 . *Earth Planet. Sci. Lett.* 230, 1–10.
- Tenner, T.J., Hirschmann, M.M., Withers, A.C., Ardia, P., 2012. H_2O storage capacity of olivine and low-Ca pyroxene from 10 to 13 GPa: consequences for dehydration melting above the transition zone. *Contrib. Miner. Petrol.* 163, 297–316.
- Troullier, N., Martins, J.L., 1991. Efficient pseudopotentials for plane-wave calculations. *Phys. Rev. B* 43, 1993–2006.
- Tsuchiya, J., Tsuchiya, T., 2009. First principles investigation of the structural and elastic properties of hydrous wadsleyite under pressure. *J. Geophys. Res.* 114, B02206.
- Tsuchiya, J., Tsuchiya, T., Tsuneyuki, S., 2005. First-principles study of hydrogen bond symmetrization of phase D under high pressure. *Am. Mineral.* 90, 44–49.
- Tsuchiya, T., Tsuchiya, J., Umemoto, K., Wentzcovitch, R.M., 2004. Phase transition in MgSiO_3 perovskite in the earth's lower mantle. *Earth Planet. Sci. Lett.* 224, 241–248.
- Umemoto, K., Wentzcovitch, R., Hirschmann, M.M., Kohlstedt, D.L., Withers, A.S., 2011. A first-principles investigation of hydrous defects and IR frequencies in forsterite: the case for Si vacancies. *Am. Mineral.* 96, 1475–1479.
- Verma, A.K., Karki, B.B., 2009. Ab initio investigations of native and protonic point defects in Mg_2SiO_4 polymorphs under high pressure. *Earth Planet. Sci. Lett.* 285, 140–149.
- Weidner, D., Sawamoto, H., Sasaki, S., Kumazawa, M., 1984. Elasticity of Mg_2SiO_4 spinel. *J. Geophys. Res.* 89, 7852–7860.
- Williams, Q., Hemley, R.J., 2001. Hydrogen in the deep Earth. *Annu. Rev. Earth Planet. Sci.* 29, 365–418.
- Wookey, J., Stackhouse, S., Kendall, J.-M., Brodholt, J., Price, G.D., 2005. Efficacy of the post-perovskite phase as an explanation for lowermost mantle seismic properties. *Nature* 438, 1004–1007.
- Zhang, L., Meng, Y., Dera, P., Yang, W., Mao, W.L., Mao, H.-K., 2013. Single-crystal structure determination of $(\text{Mg}, \text{Fe})\text{SiO}_3$ postperovskite. *Proc. Natl. Acad. Sci.* 110, 6292–6295.